Pergamon

Int. J. Heat Mass Transfer. Vol. 39, No. 8, pp. 1591–1602, 1996

0017-9310/96 $15.00+0.00

0017-9310(95)00260-X

The inviscid stagnation–flow solidification problem

R. H. RANGEL and X. BIAN

Department of Mechanical and Aerospace Engineering, University of California, Irvine, CA 92717, U.S.A.

(*Received* 7 *November* 1994 *and in final form* 6 *July* 1995)

Abstract—The stagnation–flow Stefan solidification problem is defined and investigated. By applying the method of instantaneous similarity, the temperature field, the solid–liquid interface location and its growth rate, valid for the initial stages of solidification, are obtained. Furthermore, with the use of the quasi-steady approximation, a solution of the problem valid for the final stages of solidification is obtained. The analysis reveals a fundamental difference between the stagnation–flow solidification behavior and that in the classical Stefan solidification problem. Both methods of solution are used to show that the solidification front grows asymptotically to a finite maximum value as time goes to infinity. For large values of time, both methods yield the same temperature distribution and the same value of the solid phase thickness, which are independent of the Stefan number.

1. INTRODUCTION

Transient heat transfer problems involving melting or solidification are important in many engineering applications, such as processes of casting, welding and spray forming. The last application offers the unique opportunity to combine the benefits associated with fine-particulate technique with *in situ* processing. Mathematically, the problem of solid–liquid phase change belongs to the class of moving boundary problems, because of the existence of a moving interface. In many situations involving phase change problems, multidimensional variations are important, boundary conditions are complex, thermo-physical properties vary with temperature and phase, and several mechanisms of heat transfer may take place. Thus, analytical solutions have been obtained only in a limited number of cases and investigations on phase change problems are usually conducted by numerical methods.

Examples of analytical or semi-analytical solutions to phase change problems are those of Cho and Sunderland [1] and Madejski [2]. An extensive review of analytical and numerical techniques can be found in Alexiades and Solomon [3] and Salcudean and Abdullah [4], and a review of the methods used in droplet solidification was presented by Bennett and Poulikakos [5]. The most classical exact solution is probably the so called Neumann solution of the Stefan problem [6–8] which predicts the temperature distribution and rate of solidification (or melting) of a semi-infinite medium. A significant number of numerical techniques have been developed to solve solid–liquid phase change problems [9–17]. The numerical methods used can be conveniently divided into two groups. In the first group, known as the enthalpy method, enthalpy and temperature are used as dependent variables in the energy equation. The resulting equation is applicable in both the solid and liquid regions as well as the solid–liquid interface. The location of the phase change interface is determined from the calculated enthalpy, rather than from the solid–liquid interface energy equation [9–11]. In the second group, the temperature and the solid–liquid interface location are the dependent variables and the energy conservation equations are written separately for the solid and the liquid regions. The major difficulty with this technique arises from the need to track a continuously moving phase change interface. The rate of propagation of this boundary into the liquid region (solidification) or into the solid (melting) region depends on the thermal properties of the solid and liquid regions, and in addition, in the cases where there exists motion in the liquid phase, such as metal droplet solidification in spray processes, it also depends on the fluid properties of the liquid region. Various procedures have been developed to deal with this problem [12, 13], but most of them have addressed the cases in which there is no liquid motion, or they simply have taken into account heat conduction as the sole heat transfer mechanism [5, 14]. Inspection of those investigations which have included fluid motion, such as droplet deformation and solidification during impingement on a cold substrate, indicates that despite the significant results derived from their models, the studies mainly rely on the classical Neumann solution of the Stefan solidification model to determine the solid–liquid interface position [2, 15–18]. There are several shortcomings in employing the Stefan solidification model in these cases. The most important of these is that the Stefan model corresponds to a stagnant liquid phase. An appropriate

NOMENCLATURE

A	potential flow strain
a	ratio of the liquid to solid phase thermal diffusivity
b	ratio of the liquid to solid phase thermal conductivity
c_p	specific heat
h_{sf}	latent heat of solidification
k	thermal conductivity
q''	heat flux
s	solid phase thickness
St	Stefan number
T	temperature
t	time
u	velocity component of liquid phase in x direction
v	velocity component of liquid phase in y direction
x	spatial coordinate normal to the substrate
y	spatial coordinate parallel to the substrate.

Greek symbols

α	thermal diffusivity
η	transformed coordinate
θ	nondimensional temperature
ρ	density
λ	solidification parameter
τ	nondimensional time.

Subscripts

i	initial
ℓ	liquid phase
0	substrate
m	melting
s	solid phase.

Superscript

~	nondimensional.

heat transfer and solidification model must account for convective effects due to fluid motion, and in some cases for viscous dissipation effects. In order to relax some of those limitations, the present study reports an investigation of the effect of fluid motion in the solidification problem in a half space. The solution should provide a more reasonable model for the solidification behavior of the liquid in motion, and provide better insight into situations, such as those encountered during the deformation and solidification of a droplet impinging on a cold substrate.

We investigate the effect of the liquid motion on its solidification behavior by considering the inviscid two-dimensional stagnation flow onto a cold substrate. We assume that the physical properties are independent of temperature. By coupling the conductive–convective liquid energy equation with the heat conduction equation in the solid region as well as the energy balance equation at the interface, we set up the mathematical model of the half space convective Stefan problem. An instantaneous similarity method and a quasi-steady approximation are employed to solve the time depending system of equations. A parametric study is included in the discussion of the solidification behavior. Temperature distributions are obtained, and the behavior of the solid–liquid interface location is investigated. A numerical solution of the problem is given elsewhere [19].

2. MATHEMATICAL FORMULATION

2.1. *The classical Stefan problem*

The physical description of the classical Stefan solidification problem is given as follows: a liquid at an initially uniform temperature T_i which is higher than the melting temperature T_m of the substance is confined to a half space $x > 0$. At $t = 0$, the boundary surface at $x = 0$ is lowered to a temperature T_0 below T_m and maintained at that temperature for times $t > 0$. As a result, solidification starts at the surface $x = 0$ and the solid–liquid interface moves in the positive x direction. Figure 1 illustrates the problem and shows typical temperature profiles.

The heat conduction equation for the solid phase is

$$\frac{\partial^2 T_s}{\partial x^2} = \frac{1}{\alpha_s}\frac{\partial T_s}{\partial t} \quad \text{in } 0 < x < s(t) \quad t > 0 \tag{1}$$

with the boundary condition: $T_s(x, t) = T_0$ at $x = 0$, $t > 0$.

The heat conduction equation for the liquid phase is

$$\frac{\partial^2 T_\ell}{\partial x^2} = \frac{1}{\alpha_\ell}\frac{\partial T_\ell}{\partial t} \quad \text{in } s(t) < x < \infty \quad t > 0 \tag{2}$$

with $T_\ell(x, t) \to T_i$ as $x \to \infty$, $t > 0$,
and $T_\ell(x, t) = T_i$ for $t = 0$ and $x > 0$.

The coupling conditions at the interface $x = s(t)$ are

$$T_s(x, t) = T_\ell(x, t) = T_m \tag{3}$$

$$k_s\frac{\partial T_s}{\partial x} - k_\ell\frac{\partial T_\ell}{\partial x} = \rho h_{sf}\frac{ds(t)}{dt}. \tag{4}$$

The Neumann solution of this problem is [6–8]

$$\frac{T_s(x, t) - T_0}{T_m - T_0} = \frac{\operatorname{erf}[x/2(\alpha_s t)^{1/2}]}{\operatorname{erf}(\lambda/2)} \tag{5}$$

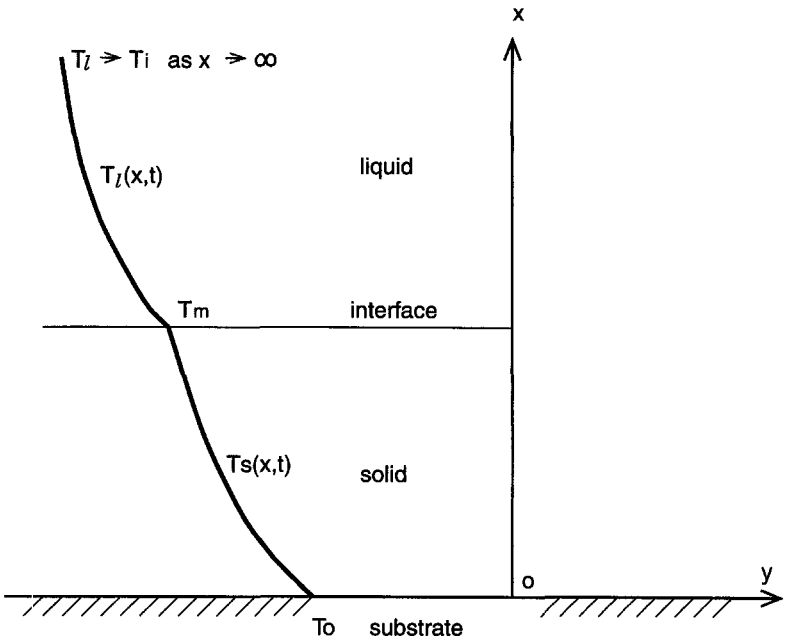

Fig. 1. Solidification in a half space: the classical Stefan solidification problem.

$$\frac{T_\ell(x,t)-T_i}{T_m-T_i}=\frac{\operatorname{erfc}\left[x/2(\alpha_\ell t)^{1/2}\right]}{\operatorname{erfc}\left(\lambda/2a^{1/2}\right)}, \tag{6}$$

where $a=\alpha_\ell/\alpha_s$. The interface is located at

$$s(t)=\lambda\sqrt{\alpha_s t}, \tag{7}$$

where λ is a parameter independent of time and determined from the following relation obtained from equation (4):

$$\frac{e^{-\lambda^2/4}}{\operatorname{erf}(\lambda/2)}+\frac{b}{a^{1/2}}\frac{T_m-T_i}{T_m-T_0}\frac{e^{-\lambda^2/4a}}{\operatorname{erfc}\left[\lambda/2a^{1/2}\right]}=\frac{\lambda\sqrt{\pi}}{2St}, \tag{8}$$

where $b=k_\ell/k_s$, and

$$St=\frac{c_{ps}(T_m-T_0)}{h_{sf}} \tag{9}$$

is the Stefan number.

2.2. *The stagnation–flow solidification problem*

We now consider the case of a stagnation flow in a half space (Fig. 2). In general, the solution for the flow field is coupled with the thermal-field solution. If the physical properties are assumed independent of temperature, the fluid mechanics and thermal solutions are still coupled because of the rising solid front. In general, the unsteady, viscous Navier–Stokes equation must be solved. If the flow is assumed inviscid, only Laplace's equation for the velocity potential needs to be solved. In this case, the unsteady fluid mechanics solution is indeed a quasi-steady solution given by

$$u=-2A(x-s(t)) \tag{10}$$

$$v=2Ay. \tag{11}$$

We note here that the inviscid assumption is most appropriate for fluids with very small Prandtl numbers, such as liquid metals. Neglecting viscous dissipation (inviscid flow), the energy equation of the liquid phase can be written as

$$\frac{\partial T_\ell}{\partial t}+u\frac{\partial T_\ell}{\partial x}+v\frac{\partial T_\ell}{\partial y}=\alpha_\ell\left[\frac{\partial^2 T_\ell}{\partial x^2}+\frac{\partial^2 T_\ell}{\partial y^2}\right]. \tag{12}$$

A straightforward scaling analysis shows that the tangential and perpendicular velocity components are of the same order of magnitude. Moreover, the tangential temperature gradient is much smaller than the normal temperature gradient. Recognizing this, the liquid phase energy equation is simplified to

$$\frac{\partial T_\ell}{\partial t}-2A(x-s(t))\frac{\partial T_\ell}{\partial x}=\alpha_\ell\frac{\partial^2 T_\ell}{\partial x^2}. \tag{13}$$

On the other hand, the solid phase energy equation equation (1), interface energy balance equation equation (4), initial and boundary conditions remain unchanged.

3. QUASI-STEADY SOLUTION

In the classical Stefan problem, the solid front moves with a velocity proportional to the square root

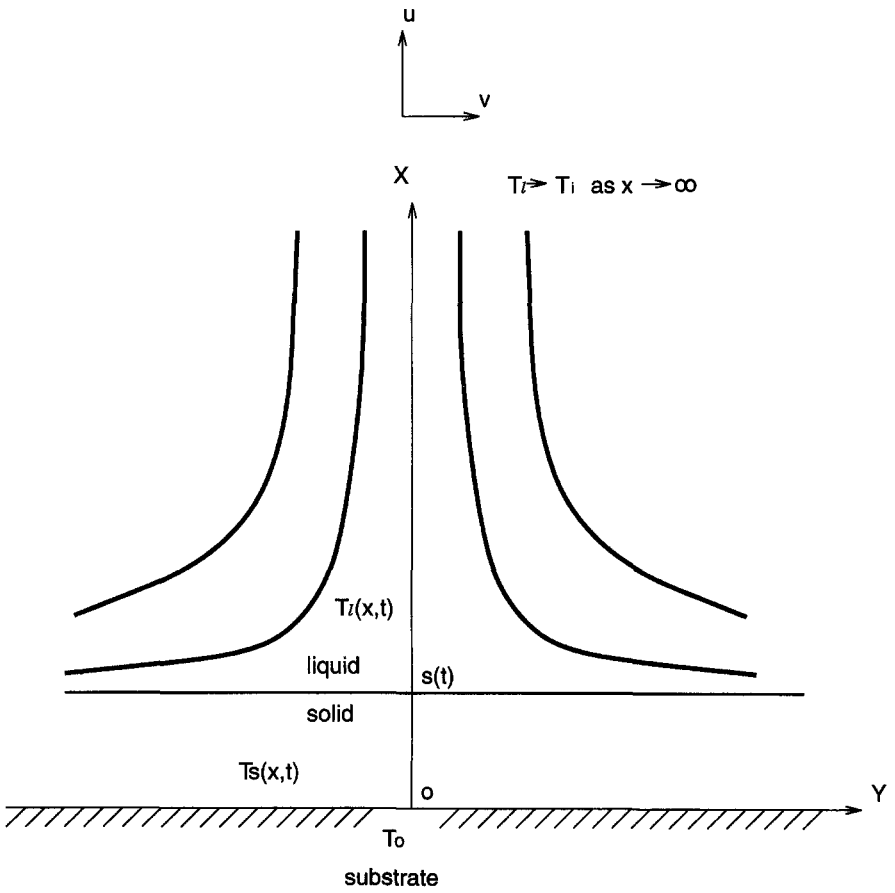

Fig. 2. Solidification in a half space: the stagnation flow solidification problem.

of time. As time approaches infinity, the velocity of the solidification front approaches zero. The same behavior is expected in the convective solidification problem. Therefore, a quasi-steady solution is expected for large values of times. In employing the quasi-steady approximation, we neglect the time derivative in the governing equations (1) and (13). The boundary and initial conditions remain unchanged.

The solid phase equation becomes

$$\frac{\partial^2 T_s}{\partial x^2} = 0 \tag{14}$$

with the solution

$$\theta_s = \frac{T_s - T_m}{T_m - T_0} = -1 + \frac{x}{s(t)}. \tag{15}$$

The liquid phase equation is

$$-2A(x - s(t))\frac{\partial T_\ell}{\partial x} = \alpha_\ell \frac{\partial^2 T_\ell}{\partial x^2} \tag{16}$$

with the solution

$$\theta_\ell = \frac{T_\ell - T_m}{T_i - T_m} = \frac{\int_s^x \exp\left[-\frac{2A}{\alpha_\ell}\left(\frac{x'^2}{2} - sx'\right)\right]dx'}{\int_s^\infty \exp\left[-\frac{2A}{\alpha_\ell}\left(\frac{x'^2}{2} - sx'\right)\right]dx'}. \tag{17}$$

The energy balance [equation (4)] can be written as

$$\rho h_{sf}\frac{ds}{dt} = \frac{k_s(T_m - T_0)}{s} - \frac{k_\ell(T_i - T_m)\exp\left(\frac{As^2}{\alpha_\ell}\right)}{\int_s^\infty \exp\left[-\frac{2A}{\alpha_\ell}\left(\frac{x'^2}{2} - sx'\right)\right]dx'}. \tag{18}$$

Employing the error function, equation (18) can be simplified to

$$\rho h_{sf}\frac{ds}{dt} = \frac{k_s(T_m - T_0)}{s} - 2(T_m - T_0)\theta_i k_\ell \sqrt{\frac{A}{\pi\alpha_\ell}} \tag{19}$$

which can be rewritten in dimensionless form as

$$\frac{1}{St}\frac{d\tilde{s}}{d\tau}=\frac{1}{\tilde{s}}-\frac{2b\theta_i}{\sqrt{a\pi}} \tag{20}$$

after introducing the dimensionless variables

$$\tilde{s}=s\sqrt{\frac{A}{\alpha_s}} \tag{21}$$

$$\tau=At. \tag{22}$$

The asymptotic value of $\tilde{s}$ can now be obtained by using the fact that $d\tilde{s}/d\tau \to 0$ as $\tau \to \infty$.

Then equation (20) gives

$$\frac{1}{\tilde{s}}-\frac{2b\theta_i}{\sqrt{a\pi}}\to 0 \quad \text{as}\ \tau\to\infty \tag{23}$$

that is

$$\tilde{s}\to\frac{\sqrt{a\pi}}{2b\theta_i} \quad \text{as}\ \tau\to\infty. \tag{24}$$

Integrating equation (20) and employing this last result yields

$$\tau=-\frac{\sqrt{a\pi}}{2b\theta_i St}\left[\frac{\sqrt{a\pi}}{2b\theta_i}\ln\left(1-\frac{2b\theta_i\tilde{s}}{\sqrt{a\pi}}\right)+\tilde{s}\right]. \tag{25}$$

Equation (24) demonstrates that there exists an upper limit of the solid phase thickness as time goes to infinity. This finding represents a significant difference between the stagnation flow and the classical solidification problems. Note also that the maximum solid thickness is independent of the Stefan number. Further discussion of this behavior is provided in the Results section.

4. SOLUTION BY THE METHOD OF INSTANTANEOUS-SIMILARITY

A classical method for solving thermal boundary-layer problems is the method of local-similarity. An especially attractive feature of the local-similarity method is that the solution at a particular streamwise location can be found without having to perform calculations at upstream locations, that is, each solution is locally autonomous. Furthermore, the governing partial-differential equations may be transformed into ordinary differential equations with more straightforward solutions.

Here, the concept of local-similarity is applied to the time variation of the liquid phase temperature. Strictly speaking, it should be referred to as an instantaneous-similarity method to differentiate it from the local-similarity, which refers to a similarity in space. Mathematically, however, the solution proceeds in an analogous manner.

Firstly, the new variables (η, τ) are introduced and the coordinates (x, t) are transformed to (η, τ), where

$$\eta=\frac{x}{\sqrt{\alpha_s t}} \tag{26}$$

$$\tau=At. \tag{27}$$

At the same time, the temperature is changed to the dimensionless form

$$\theta=\frac{T-T_m}{T_m-T_0}. \tag{28}$$

The governing equations are transformed to:

Solid phase [equation (1)],

$$\tau\frac{\partial\theta_s}{\partial\tau}=\frac{\partial^2\theta_s}{\partial\eta^2}+\tfrac{1}{2}\eta\frac{\partial\theta_s}{\partial\eta} \tag{29}$$

with $\theta_s=-1$ at $\eta=0$, and $\theta_s=0$ at $\eta=s(t)/\sqrt{\alpha_s t}=\lambda$.

Liquid phase [equation (13)],

$$\tau\frac{\partial\theta_\ell}{\partial\tau}=[2\tau(\eta-\lambda)+\tfrac{1}{2}\eta]\frac{\partial\theta_\ell}{\partial\eta}+a\frac{\partial^2\theta_\ell}{\partial\eta^2} \tag{30}$$

with $\theta_\ell=0$ at $\eta=\lambda$ and $\theta_\ell\to\theta_i$ at $\tau=0$ or $\eta\to\infty$.

The energy balance at the interface location [equation (4)] becomes

$$b\frac{\partial\theta_\ell}{\partial\eta}+\frac{\lambda}{2St}+\frac{\tau}{St}\frac{d\lambda}{d\tau}=\frac{\partial\theta_s}{\partial\eta} \quad \text{at}\ \eta=\lambda. \tag{31}$$

In accordance with the instantaneous similarity assumptions, we neglect terms involving derivatives with respect to τ and integrate the remaining ordinary differential equations. The results are expected to be valid for small values of τ, but as will be shown below, they are also valid for large values of τ. The solid phase temperature distribution is

$$\theta_s=-1+\frac{\operatorname{erf}(\eta/2)}{\operatorname{erf}(\lambda/2)} \tag{32}$$

while the liquid phase temperature distribution is

$$\theta_\ell=\theta_i\frac{\displaystyle\int_\lambda^\eta \exp\left[-\frac{(1/4+\tau)}{a}\eta'^2+\frac{2\lambda\tau}{a}\eta'\right]d\eta'}{\displaystyle\int_\lambda^\infty \exp\left[-\frac{(1/4+\tau)}{a}\eta'^2+\frac{2\lambda\tau}{a}\eta'\right]d\eta'}. \tag{33}$$

The interface energy balance equation becomes

$$\frac{\exp(-\lambda^2/4)}{\sqrt{\pi}\operatorname{erf}(\lambda/2)}-\frac{\lambda}{2St}=\frac{b\theta_i\exp\left[-(\tfrac{1}{4}-\tau)\dfrac{\lambda^2}{a}\right]}{\displaystyle\int_\lambda^\infty \exp\left[-\frac{(1/4+\tau)}{a}\eta'^2+\frac{2\lambda\tau}{a}\eta'\right]d\eta'} \tag{34}$$

from which λ can be determined. By employing the error function, equation (34) can be rewritten as

$$\frac{\exp(-\lambda^2/4)}{\sqrt{\pi}\,\mathrm{erf}(\lambda/2)} - \frac{\lambda}{2St}$$

$$= \frac{\theta_i b}{\sqrt{\pi}} \frac{\sqrt{\frac{(1+4\tau)}{a}}\exp\left[-\frac{\lambda^2}{4a(1+4\tau)}\right]}{\mathrm{erfc}\left[\frac{\lambda}{\sqrt{4a(1+4\tau)}}\right]}. \quad (35)$$

Equation (35) shows that λ is a function of time, in contrast with the λ of the classical Stefan problem which is independent of time. It should also be noted that equation (35) reduces to the corresponding one for the stagnant case [equation (8)] for $\tau = 0$. Equation (35) is evaluated numerically to determine the time variation of the solidification front $\tilde{s} = \lambda\sqrt{\tau}$.

The existence of an asymptotic upper limit for $\tilde{s}$ can also be shown from the instantaneous-similarity results. We first obtain the limit of λ as $\tau \to \infty$ from equation (35)

$$\lambda \to \frac{\sqrt{a\pi}}{2b\theta_i\sqrt{\tau}} \quad \text{as } \tau \to \infty \quad (36)$$

which yields

$$\tilde{s} \to \frac{\sqrt{a\pi}}{2b\theta_i} \quad \text{as } \tau \to \infty \quad (37)$$

corresponding to the same result, equation (24), obtained in the quasi-steady analysis. This is an indication of the validity of the instantaneous similarity method for large values of time. This fact becomes evident when one observes that all terms involving time derivatives in the governing equation in the (τ, η) space are of the form $\tau(\partial/\partial\tau)$ which is small for the initial times ($\tau \to 0$). For large times, the term $\partial/\partial\tau$ can be neglected after dividing the governing equations by τ and taking the limit for $\tau \to \infty$ ($t \to \infty$). This last procedure is in fact equivalent to a quasi-steady approximation.

5. RESULTS

Figure 3 shows the variation of λ with St for different values of τ for the cases of (a) $\theta_i = 1, a = 1, b = 1$; (b) $\theta_i = 1, a = 0.5, b = 0.5$; (c) $\theta_i = 0.1, a = 1, b = 1$; (d) $\theta_i = 10, a = 1, b = 1$. It can be seen that for the same St, λ decreases as τ increases, while for the same τ, λ increases with increasing St. Figure 4 shows the variation of λ with St at an early time for the above four cases of θ_i, a, b. It can be seen that during the initial stages of solidification ($\tau = 0.1$) and for a very small Stefan number, the values of λ are very similar for all cases. On the other hand, for a large Stefan number, there are significant differences in λ for the different cases, with smaller values of θ_i, a and b corresponding to larger values of λ, as expected. It can also been seen that as θ_i increases to 10, λ remains almost independent of the Stefan number.

Figure 5a shows the variation of λ with τ for different values of St for the case of $\theta_i = 1$, $a = 1$ $b = 1$. It should be noted that λ approaches 0 as τ approaches infinity. For small values of τ, that is, during the initial stages of solidification, λ decreases faster for larger values of the St number, and larger values of the Stefan number correspond to higher λ. In Fig. 5b, a comparison is made of the variation of λ with τ for the four cases of (a) $\theta_i = 1$, $a = 1$ $b = 1$; (b) $\theta_i = 1$, $a = 0.5, b = 0.5$; (c) $\theta_i = 0.1, a = 1$ $b = 1$; (d) $\theta_i = 10$, $a = 1$ $b = 1$ for a Stefan number of 1. It can be seen that for the same value of the Stefan number, smaller values of θ_i, a and b correspond to higher value of λ.

An estimate of the accuracy of the instantaneous similarity method is obtained by calculating the magnitude of the term $\tau(\partial\theta/\partial\tau)$ for the solid phase. From the solution of the solid phase temperature, equation (32), we obtain

$$\frac{\partial\theta_s}{\partial\tau} = -\frac{\mathrm{erf}(\eta/2)\,e^{-\lambda^2/4}\frac{1}{\sqrt{\pi}}\frac{d\lambda}{d\tau}}{(\mathrm{erf}(\lambda/2))^2}. \quad (38)$$

The maximum value of $\partial\theta_s/\partial\tau$ is at $\eta = \lambda$, where

$$M = \left.\frac{\partial\theta_s}{\partial\tau}\right|_{\eta=\lambda} = -\frac{\frac{1}{\sqrt{\pi}}e^{-\lambda^2/4}\frac{d\lambda}{d\tau}}{\mathrm{erf}(\lambda/2)}. \quad (39)$$

Figure 6a shows the variation of τM with τ for different values of St for the case of $\theta_i = 1$, $a = 1$, $b = 1$. It can be seen that during the initial stages of solidification, the value of τM is small enough to ensure the accuracy of the local similarity solution. In Fig. 6b, a comparison is made of the variation of τM with τ for a fixed Stefan number for the four cases (a) $\theta_i = 1$, $a = 1$, $b = 1$; (b) $\theta_i = 0.1$, $a = 1$, $b = 1$; (c) $\theta_i = 1$, $a = 0.5$, $b = 0.5$; (d) $\theta_i = 10$, $a = 1$, $b = 1$. It can be seen that for all cases, the value of τM is small in the initial stages of solidification, particularly for smaller a, b and θ_i.

Figure 7a shows the variation of the dimensionless thickness $\tilde{s}$ with τ for different values of the Stefan number for the case of $\theta_i = 1$, $a = 1$, $b = 1$ calculated from the instantaneous similarity results. It can be seen that $\tilde{s}$ increases with τ, and that there exists an upper limit of $\tilde{s}$ as τ approaches infinity, equation (37). It can also be observed that this limit value is independent of the Stefan number and that $\tilde{s}$ increases faster for larger St. Figure 7b shows a comparison of the variation of $\tilde{s}$ with τ for four cases (a) $\theta_i = 1$, $a = 1$, $b = 1$; (b) $\theta_i = 0.1$, $a = 1$, $b = 1$; (c) $\theta_i = 1$, $a = 0.5, b = 0.5$; (d) $\theta_i = 10, a = 1, b = 1$ for the same Stefan number. The dimensionless thickness $\tilde{s}$ increases faster for smaller a, b and θ_i.

Figure 8a shows the temperature distribution along the nondimensional x coordinate,

$$\tilde{x} = x\sqrt{\frac{A}{\alpha_s}} = \eta\sqrt{\tau}$$

during the initial and final stages of solidification

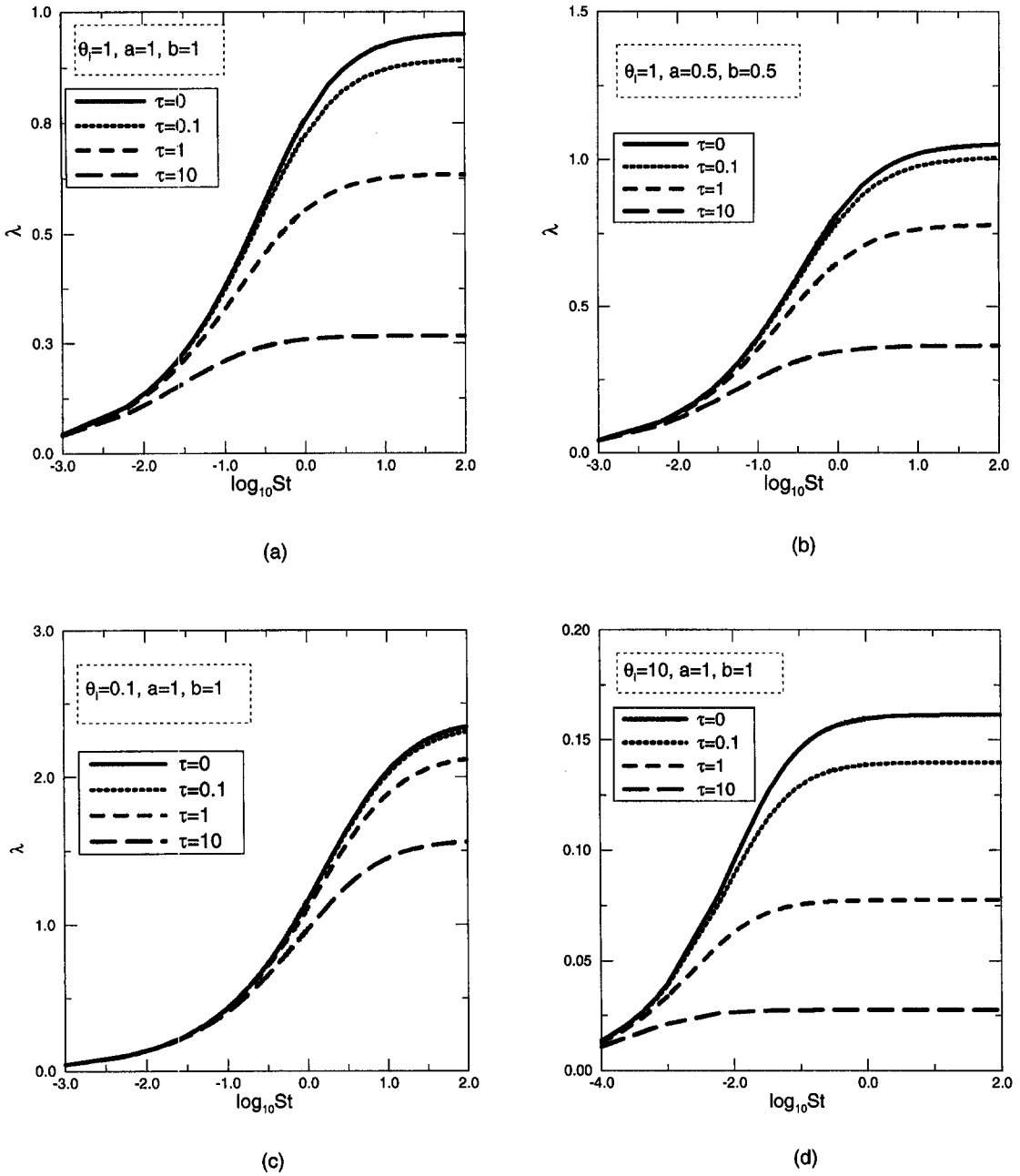

Fig. 3. Variation of λ with Stefan number for different solidification times.

obtained with the instantaneous similarity method. It can be seen that at very large time, the temperature distribution becomes independent of the Stefan number. Figure 8b shows the temperature distribution during the initial stages of solidification ($\tau = 0.1$) and at very large time ($\tau = 100$) for the cases of (a) $\theta_i = 1$, $a = 1$, $b = 1$; (b) $\theta_i = 0.5$, $a = 1$, $b = 1$ and (c) $\theta_i = 1$, $a = 0.5$, $b = 0.5$. During the initial stages of solidification and at the same position in the liquid phase, the liquid temperature is lower for higher a and b, as expected. For large time, however, at the same position in the liquid phase or solid phase, the temperature θ_ℓ or θ_s is lower for the cases with lower a, b or θ_i. Thus, it can be concluded that variations in Stefan number bring about changes in the temperature distribution and interface location in the initial stage of solidification, while changes in the parameters θ_i, a and b affect both the initial stage and the long time behavior of the solution.

The two solutions obtained from equations (34) and

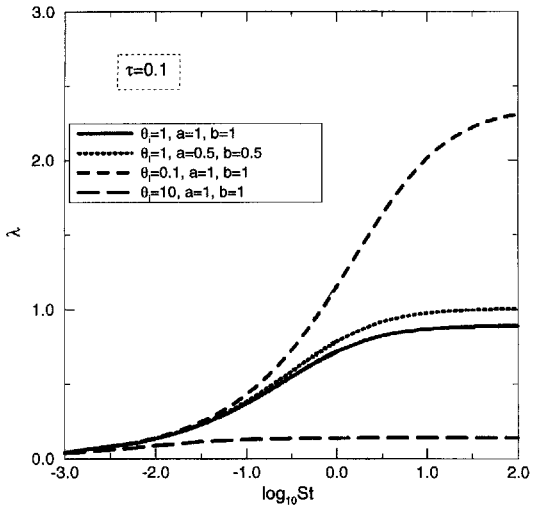

Fig. 4. Variation of λ with Stefan number at the initial stage of solidification.

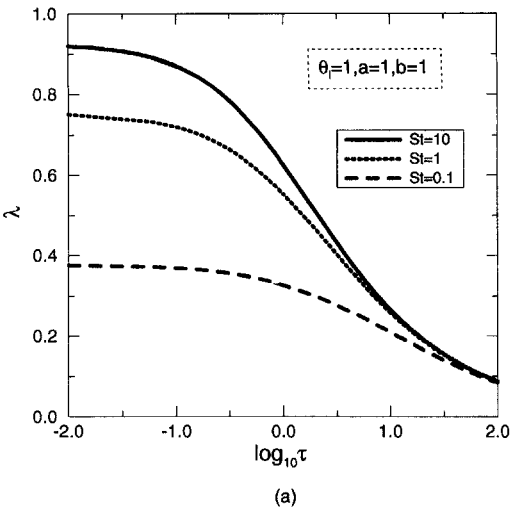

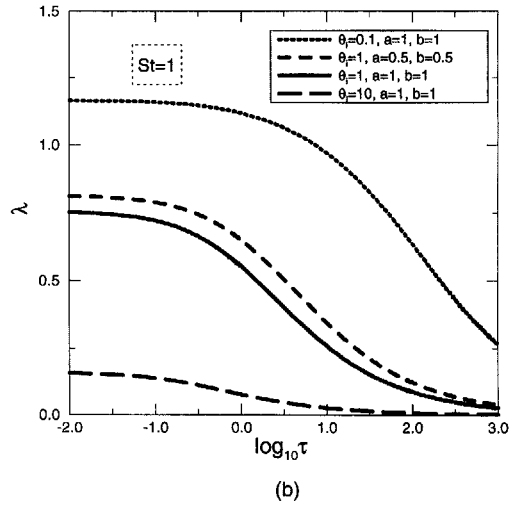

Fig. 5. Variation of λ with time: (a) effect of Stefan number, (b) effect of θ_i, a and b.

(25), corresponding to the instantaneous similarity solution and the quasi-steady approximation, respectively, are compared in Fig. 9. In Fig. 9a, the variation of the solid phase thickness $\tilde{s}$ with time τ is plotted for different Stefan numbers for the case of $\theta_i = 1$, $a = 1$, $b = 1$. The interface location obtained from the quasi-steady solution approaches the upper limit much faster than that obtained from the method of instantaneous similarity. It should be noted that the difference between the solutions is diminished as the Stefan number is made smaller. A comparison of the two solutions for the cases of (a) $\theta_i = 0.1$, $a = 1$, $b = 1$; (b) $\theta_i = 1$, $a = 0.5$, $b = 0.5$; (c) $\theta_i = 1$, $a = 1$, $b = 1$ and (d) $\theta_i = 10$, $a = 1$, $b = 1$ is made in Fig. 9b. It can be seen that both methods predict the same upper limit as time approaches infinity.

Figure 10a shows the quasi-steady temperature distributions in the initial and final stages of solidification for various Stefan numbers for the case $\theta_i = 1$, $a = 1$ and $b = 1$. The qualitative behavior of the solutions is similar to that of the instantaneous similarity solutions, although there are quantitative differences. Figure 10b shows the quasi-steady the temperature distributions for the cases of (a) $\theta_i = 1$, $a = 1$, $b = 1$; (b) $\theta_i = 0.5$, $a = 1$, $b = 1$ and (c) $\theta_i = 1$, $a = 0.5$, $b = 0.5$ with a Stefan number of 1.

A comparison of the temperature distributions obtained with the instantaneous similarity solution and with the quasi-steady approximation in the initial stage of solidification and at very large solidification times is shown in Fig. 11. During the initial stages of solidification, the solid phase thickness growth rate obtained with the quasi-steady solution is higher than that computed with the instantaneous similarity solution. Because it neglects the transient cooling of both the liquid and solid phases, the quasi-steady solution predicts a faster solidification rate. On the other hand, during the final stages of solidification, both solutions approach one another. In fact, a scaling analysis shows that as $\tau \to \infty$, the governing equations (29) and (30) used to derive the instantaneous similarity solution of the solid and liquid phase temperature distributions, have the same form as equation (14) and equation (16), respectively. Considering this fact and that both methods predict the same upper limit of interface location, it can be concluded that the instantaneous similarity solution is valid for both the initial and final stages of solidification. On the other hand, the quasi-steady approximation is simpler, but only valid for the long time behavior of the problem. The intermediate time behavior could only be obtained with a numerical solution.

The existence of a finite asymptotic limit for the

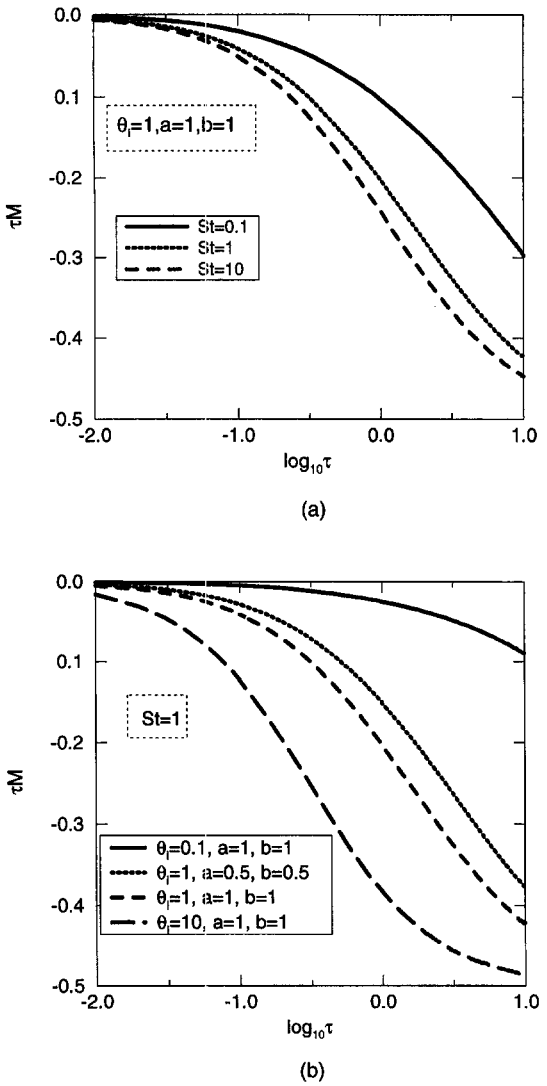

Fig. 6. Evaluation of the instantaneous similarity method.

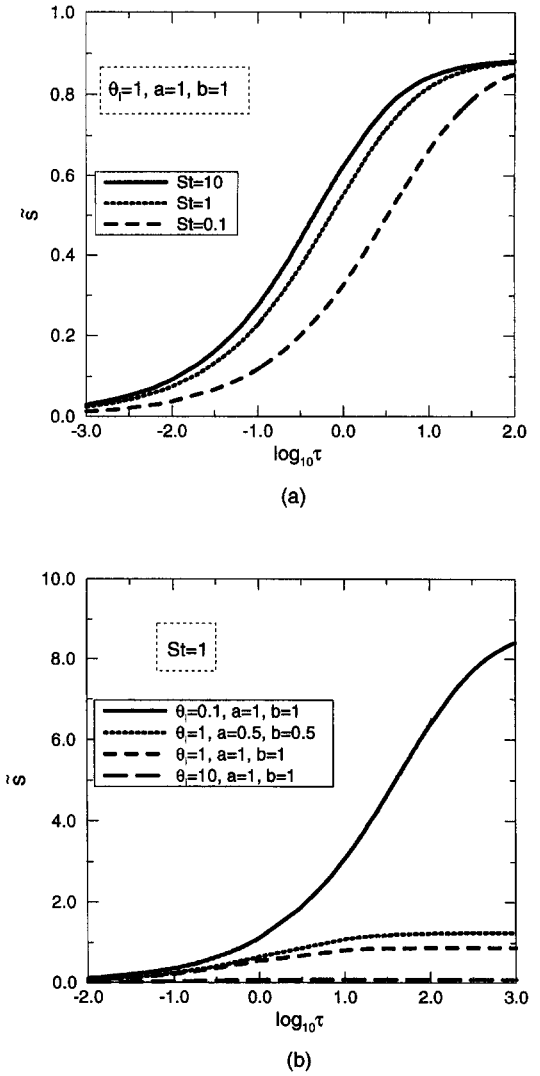

Fig. 7. Temporal growth of the solid phase obtained by instantaneous similarity: (a) effect of Stefan number, (b) effect of θ_i, a and b.

solidification front in the stagnation–flow problem may be understood with the aid of Fig. 12, by realizing that the thermal field in the liquid phase reaches a truly quasi steady solution after a finite time. This implies that the heat flux at the interface on the liquid side decreases, not to zero, but to a finite value in the limit of $t \to \infty$. This is not the case in the classical Stefan solidification problem where the heat flux at the interface on the liquid side continues to decrease as $t^{-1/2}$ as $t \to \infty$. Moreover, the behavior of the heat flux at the interface on the solid side is similar for both the classical and the stagnation flow problems. In the long-time behavior, this heat flux is dictated by the conduction heat transfer through the solid

$$q_s'' \sim \frac{T_m - T_0}{s}. \tag{40}$$

In the classical problem, the solid thickness s increases as $t^{1/2}$ and thus, the solid heat flux decreases as $t^{-1/2}$, the same rate of decrease of the liquid heat flux. Since energy arriving at the interface by conduction from the liquid must ultimately be conducted through the solid into the substrate, the solid flux must be at least as large as the liquid heat flux. It is actually larger, since it must also carry the latent heat of solidification released at the interface. In the stagnation–flow solidification problem, the solid front can only rise to a height which results in a solid heat flux equal to the liquid heat flux. At that point, no further solidification is possible.

A few calculations illustrating some practical cases for aluminum and tungsten are discussed next. The initial liquid temperature is chosen as 100 K above

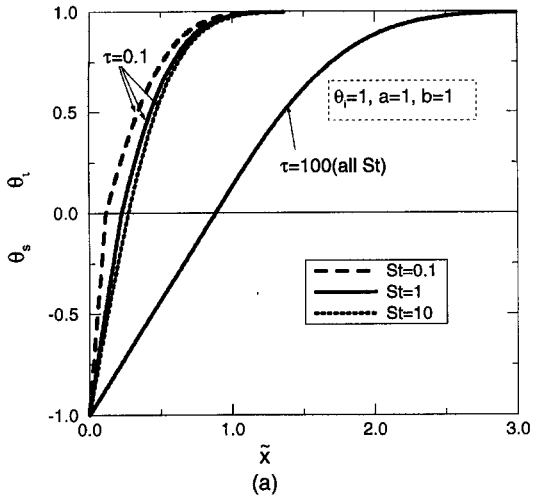

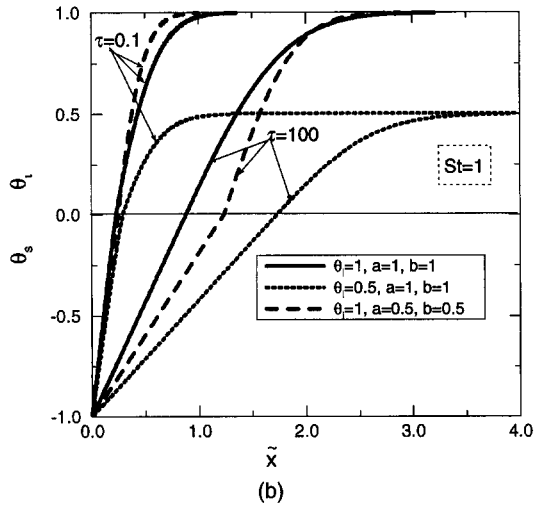

Fig. 8. Temperature distribution at different times obtained with the instantaneous similarity method: (a) effect of Stefan number, (b) effect of θ_f, a and b.

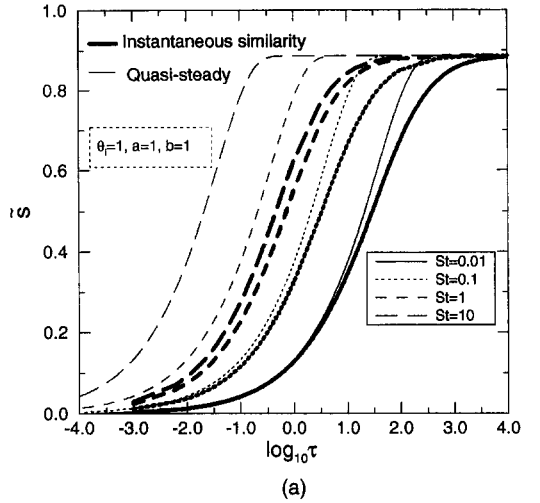

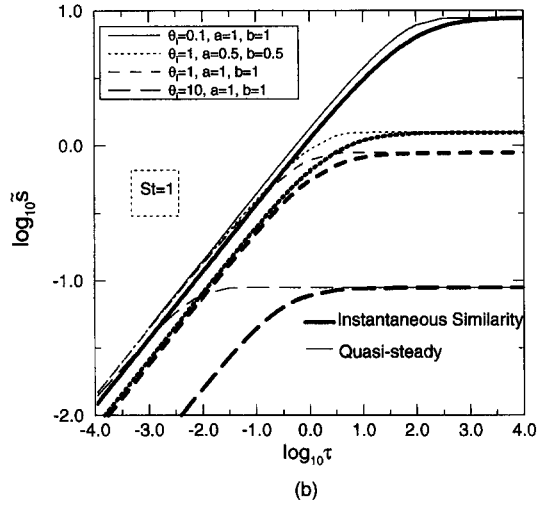

Fig. 9. Variation of the solid phase thickness with time: comparison of methods: (a) effect of Stefan number, (b) effect of θ_f, a and b.

the melting temperature. The substrate temperature is 300 K. Other parameters are given in Fig. 13 which compares the evolution of the solid front with time for the stagnation–flow solidification model, with the Neumann solution of the classical Stefan problem (without liquid motion). It can be seen that the solid front location, obtained from the instantaneous similarity method, approaches an upper limit as time increases. On the other hand, the solid front in the Neumann solution grows indefinitely with time. The effect of the liquid flow motion on its solidification behavior can also be observed in Fig. 13 by comparing the solid front evolutions corresponding to different values of the strain rate ($A = 10^3\ s^{-1}$, $10^6\ s^{-1}$, $10^7\ s^{-1}$, and $10^8\ s^{-1}$, respectively). In high speed metal spray deposition processing, the strain rate A is of the order of v/D, where v is the liquid droplet impinging velocity and D is the droplet diameter. For example, if $v = 100$ m s^{-1}, and $D = 10$ μm, the corresponding value of A would be $10^7\ s^{-1}$. It can be observed that increasing the strain rate results in a decrease of both the upper limit reached by the solidification front and the time to approach such a limit. It can also be concluded that as the strain rate is reduced to a very small value, that is, as the fluid velocity approaches zero, the stagnation flow solidification behavior coincides with the Neumann solution of the solidification problem without liquid motion.

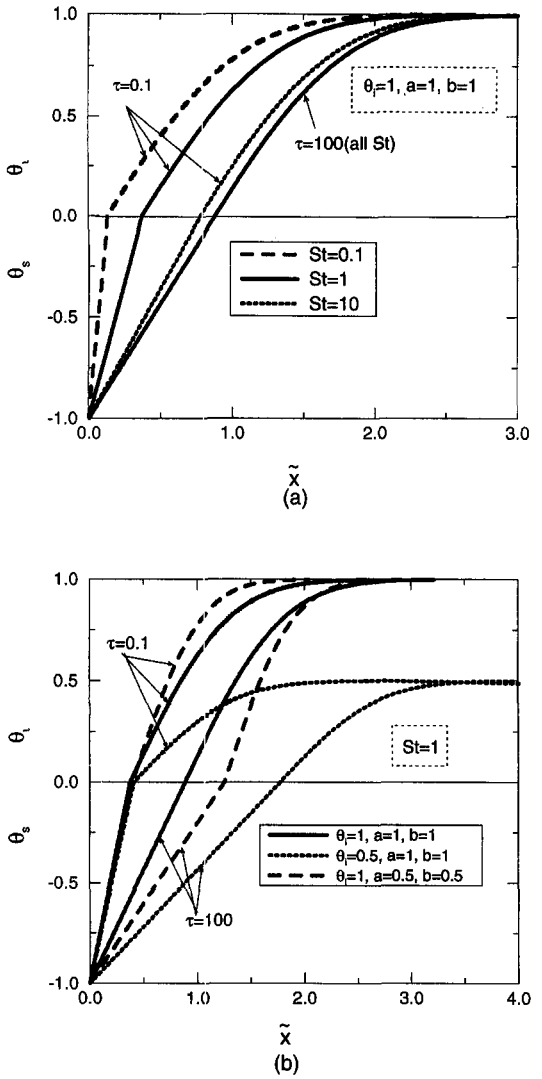

Fig. 10. Temperature distribution at different times obtained with the quasi-steady method: (a) effect of Stefan number, (b) effect of θ_i, a and b.

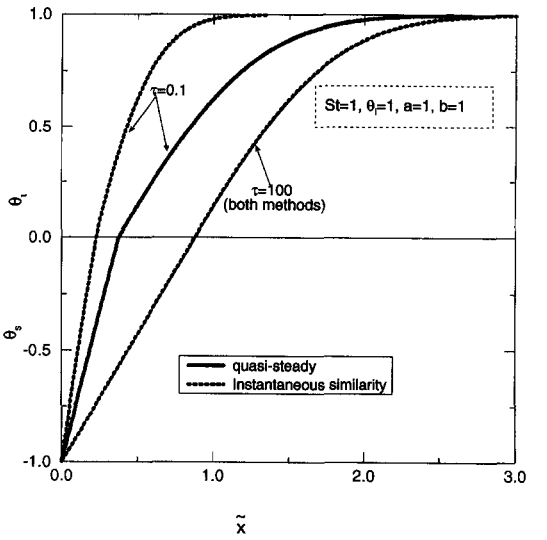

Fig. 11. Comparison of the temperature distributions obtained with the two methods.

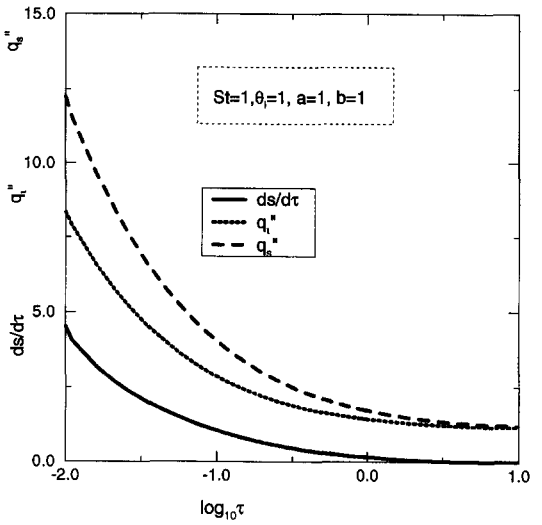

Fig. 12. The time variation of the solid and liquid heat fluxes at the interface and the solid–liquid interface growth rate.

6. CONCLUSIONS

The stagnation–flow Stefan solidification problem has been defined and both a quasi-steady approximation and the instantaneous similarity method have been used to solve it and to obtain the solid and liquid phase temperature distribution and the interface location. The results reveal important differences in the solidification behavior between the classical Stefan problem and the stagnation flow problem. When the position of the solidification front is expressed as $\tilde{s} = \lambda\sqrt{\tau}$, the analysis show that λ is a decreasing function of time, in contrast with the classical solution for the stagnant case in which λ is constant in time. In addition, λ is a function of the Stefan number, the ratio of the liquid to solid thermal conductivity, the ratio of the liquid to solid thermal diffusivity, and the dimensionless temperature ratio $\theta_i = T_i - T_m / T_m - T_0$. Both methods show that there exists an upper limit of the solid phase thickness as solidification time goes to infinity, and comparisons show that the two methods yield the same value of the upper limit of the nondimensionalized solid phase thickness. This is in contrast with the solution of the classical Stefan problem in which the solid phase thickness continues to grow with the square root of time as time goes to infinity.

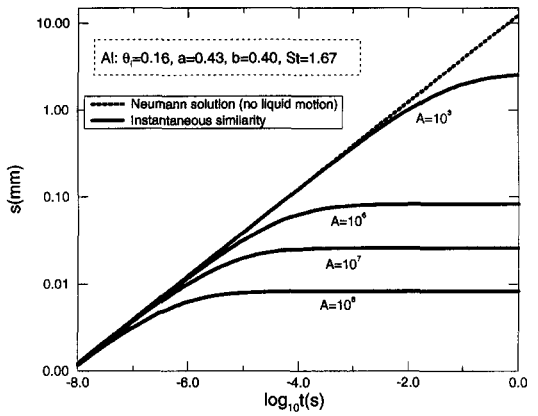

(a)

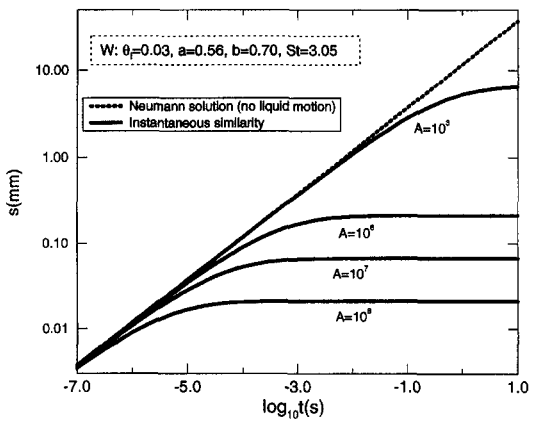

(b)

Fig. 13. Comparison of the solid-front time evolution between the stagnation–flow solidification model and the Neumann solution of the classical Stefan problem. (a) Aluminum, (b) tungsten.

Acknowledgement—This work has been supported by a grant from the National Science Foundation (CTS-9224856).

REFERENCES

1. S. H. Cho and J. E. Sunderland, Heat-conduction problems with melting or freezing, *J. Heat Transfer* **91c,** 421–426 (1969).
2. J. Madejski, Solidification of droplets on a cold surface, *Int. J. Heat Mass Transfer* **19,** 1009–1013 (1976).
3. V. Alexiades and A. D. Solomon, *Mathematical Modeling of Melting and Freezing Processes* (1st Edn), p. 210. Hemisphere, Bristol (1993).
4. M. Salcudean and Z. Abdullah, On numerical modeling of heat transfer during solidification processes, *Int. J. Numer. Meth. Engng* **25,** 445–473 (1988).
5. T. Bennett and D. Poulikakos, Splat-quench solidification: estimating the maximum spreading of a droplet impacting a solid surface, *J. Mater. Sci.* **28,** 963–970 (1993).
6. H. M. Weber, *Die partiellen Differential-Gleichungen der mathematischen Physik nach Riemann's Vorlesungen* (2nd Edn), p. 121. F. Vieweg und Sohn, Braunschweig (1912).
7. H. S. Carslaw and J. C. Jaeger, *Conduction of Heat in Solids* (2nd Edn), p. 283. Clarendon Press, London (1959).
8. M. N. Ozisik, *Heat Conduction* (1st Edn), p. 439. Wiley, New York (1980).
9. N. Shamsundar and E. M. Sparrow, Analysis of multidimensional conduction phase change via the enthalpy model, *J. Heat Transfer* **97,** 333–340 (1975).
10. M. Rappaz, Modeling of microstructure formation in solidification processes, *Int. Mater. Rev.* **34,** 93–123 (1989).
11. A. A. Rostami, R. Greif and R. E. Russo, Modified enthalpy method applied to rapid melting and solidification, *Int. J. Heat Mass Transfer* **35,** 2161–2172 (1992).
12. L. E. Goodrich, Efficient numerical technique for one dimensional thermal problems with phase change, *Int. J. Heat Mass Transfer* **21,** 615–621 (1978).
13. W. Shyy, H. S. Udaykumar and S. J. Liang, An interface tracking method applied to morphological evolution during phase change, *Int. J. Heat Mass Transfer* **36,** 1833–1844 (1993).
14. A. Y. Belekii and S. N. Zolotarev, Theoretical analysis of fluid dynamics and heat transfer in the single roller rapid solidification method, *Int. J. Rapid Solidific.* **6,** 41–54 (1991).
15. T. Watanabe, I. Kuribayashi, T. Honda and A. Kanzawa, Deformation and solidification of a droplet on a cold substrate, *Chem. Engng Sci.* **47,** 3059–3065 (1992).
16. C. San Marchi, H. Liu, E. J. Lavernia and R. H. Rangel, Numerical analysis of the deformation and solidification of a single droplet impinging onto a flat substrate, *J. Mater. Sci.* **28,** 3313–3321 (1993).
17. H. Liu, E. J. Lavernia and R. H. Rangel, Numerical simulation of substrate impact and freezing of droplets in plasma spray processes, *J. Phys. D: Appl. Phys.* **26,** 1900–1908 (1993).
18. H. Liu, E. J. Lavernia and R. H. Rangel, Numerical investigation of micropore formation during substrate impact of molten droplets in plasma spray processes, *Atomizat. Sprays* **4,** 369–384 (1994).
19. R. H. Rangel and X. Bian, Numerical solution of the inviscid stagnation–flow solidification problem, *Numer. Heat Transfer-Part A: Applications* (in press).